JOURNAL OF SPACECRAFT AND ROCKETS
Vol. 36, No. 3, May–June 1999

Aerodynamics of the Mars Microprobe Entry Vehicles

R. A. Mitcheltree,* J. N. Moss,† F. M. Cheatwood,‡ F. A. Greene,* and R. D. Braun§
NASA Langley Research Center, Hampton, Virginia 23681

The selection of the unique aeroshell shape for the Mars Microprobes is discussed. A description of its aerodynamics in hypersonic rarefied, hypersonic continuum, supersonic, and transonic flow regimes is then presented. This description is based on direct simulation Monte Carlo analyses in the rarefied flow regime, thermochemical nonequilibrium computational fluid dynamics in the hypersonic regime, existing wind-tunnel data in the supersonic and transonic regime, additional computational work in the transonic regime, and, finally, ballistic-range data. The aeroshell is shown to possess the correct combination of aerodynamic stability and drag to convert the probe's initial tumbling attitude and high velocity at atmospheric interface into the desired surface-impact orientation and velocity.

Nomenclature

A	= reference aerodynamic area, m^2
B	= ballistic coefficient, kg/m^2
C_A	= axial force coefficient
C_D	= drag force coefficient
C_m	= moment coefficient
$C_{m,\alpha}$	= slope of the moment coefficient curve, deg^{-1}
$C_{m,q} + C_{m,\dot{\alpha}}$	= dynamic derivatives, rad^{-1}
C_N	= normal force coefficient
D	= base diameter of capsule, m
Kn	= Knudsen number
M	= Mach number
M_s	= mass, kg
q	= stagnation-point heating rate, W/cm^2
R_{base}	= base radius, m
R_n	= nose radius, m
R_s	= shoulder radius, m
t	= independent variable time, s
V	= velocity, m/s
α	= angle of attack, deg
δ	= distance above stagnation point, m

Introduction

WHEN the Mars Surveyor mission is launched in February of 1999, it will transport not only its own lander and orbiter to Mars, but two small soil penetrators. These two Mars Microprobes[1] are the second of the Deep Space missions from the New Millennium Program Office. Upon arriving at Mars, the penetrators will be released from the Surveyor spacecraft and begin a free fall to the surface. This paper focuses on the aerodynamic challenges associated with that Mars entry. In particular, the penetrators must be packaged within passive aeroshells that will carry their instrumented payloads safely through hypersonic rarefied, hypersonic continuum, supersonic, and transonic flows to an impact with the surface at prescribed velocity and attitude.

Presented as Paper 97-3658 at the AIAA Atmospheric Flight Mechanics Conference, New Orleans, LA, Aug. 11–13, 1997; received Jan. 10, 1998; revision received Aug. 15, 1998; accepted for publication Feb. 22, 1999.

*Aerospace Engineer, Aerothermodynamics Branch, Aero and Gas Dynamics Division. Senior Member AIAA.
†Aerospace Engineer, Aerothermodynamics Branch, Aero and Gas Dynamics Division. Fellow AIAA.
‡Aerospace Engineer, Vehicle Analysis Branch, Space Systems and Concepts Division. Member AIAA.
§Aerospace Engineer, Vehicle Analysis Branch, Space Systems and Concepts Division. Senior Member AIAA.

The objective of this paper is to review the decisions made in the selection of the aeroshells to fulfill these requirements, and then describe in depth the expected aerodynamics in each of the flight regimes. This description is based on direct simulation Monte Carlo (DSMC) analyses in the rarefied flow regime, thermochemical nonequilibrium computational fluid dynamics (CFD) in the hypersonic regime, existing wind-tunnel data in the supersonic and transonic regime, additional CFD in the transonic regime, and, finally, ballistic-range data.

Selection of the Aeroshell

Selection of the aeroshell for Mars Microprobe requires consideration of the unique objectives of the mission. An enclosure is required that will safely deliver the penetrator payload through entry to impact with the surface. The aeroshell must decelerate the vehicle during its descent to a prescribed impact velocity. It must possess sufficient stability to correct an initial tumbling attitude to one of forward-facing flight early in the trajectory, and it must maintain that orientation within small tolerances until impact. This attitude control must be accomplished passively because there is no accommodation for active controls. Finally, the aeroshell must protect the payload from intense aerodynamic heating. The basis for this selection is discussed in the following paragraphs.

The Viking[2] and Mars Pathfinder[3] landers, as well as the Pioneer Venus[4] and Galileo[5] probes, used spherically blunted cones for their forebody. Selection of the appropriate cone angle involves tradeoffs between drag, heating, stability, and overall size. Blunter, i.e., larger half-angle, cones exhibit more drag for a given surface area as well as lower heating; sharper cones possess more stability. Both Pioneer Venus and Galileo used 45-deg half-angle cones, but these missions were entering atmospheres much denser than Mars. The two Mars missions (Viking and Pathfinder) require the higher drag properties of 70-deg sphere-cones to decelerate their heavy landers at sufficiently high altitudes to permit parachute deployment. Mars Microprobe is light (around 3 kg) and must impact the surface with sufficient speed for penetrator insertion. In addition, Microprobe requires the highest possible stability.

The impact-velocity problem can be discussed in terms of the ballistic coefficient B,

$$B = M_s / C_D A \tag{1}$$

Figure 1 compares the expected impact velocity vs ballistic coefficient for this Mars entry from three-degree-of-freedom (DOF) entry simulations. The range of acceptable impact speeds is shown in Fig. 1. For a velocity of 160 m/s, a ballistic coefficient near 28 kg/m^2 is necessary. The current mass estimate for Microprobe is 2.4 kg, and the size that can be attached to the Mars Surveyor spacecraft has diameter D of 0.325 m ($A = 0.08296$ m^2); thus, the drag coefficient must be around 1.0: the value for a 45-deg cone. (Since this work was performed, the diameter was increased to 0.35 m and the mass estimate was increased to 3.4 kg.)

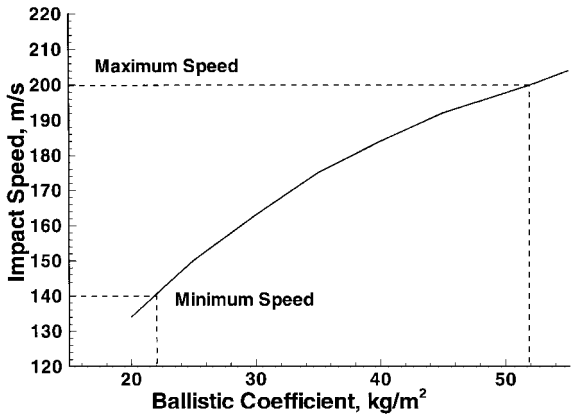

Fig. 1 Ballistic coefficient required for different impact speeds.

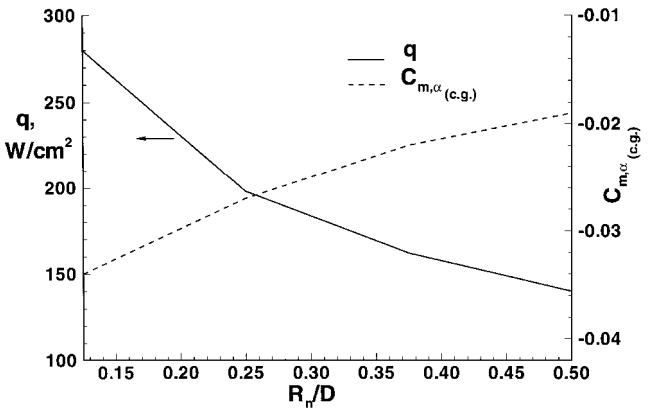

Fig. 2 Increased nose radius trade between maximum stagnation-point heating rate and transonic static stability.

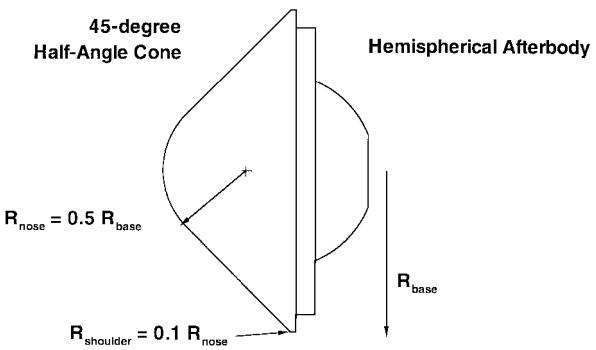

Fig. 3 Pioneer Venus small probe geometry.

The extent of spherical blunting of the nose has a minimal effect on the drag coefficient for a 45-deg half-angle cone. However, Fig. 2 reveals that increased nose bluntness decreases the maximum stagnation-point heating rate because heat rate varies as the inverse square of the effective nose radius. Unfortunately, increased nose bluntness also decreases static stability, as shown by the decreasing negative values for the slope of the moment curve ($C_{m,\alpha}$ from Mach 1.65 wind-tunnel measurements in Ref. 6). Selecting the appropriate nose bluntness is a tradeoff between heating and stability. For Microprobe, a nose radius equal to half of the overall vehicle's base radius ($R_n/D = 0.25$) is chosen. This ratio is the same used in the Pioneer Venus and Galileo probes. In an analogous manner, rounding the vehicle's shoulders decreases the heating at that location. However, rounding the shoulders decreases drag and stability. The compromise is to again use the Pioneer Venus values: shoulder radius R_s equal to $\frac{1}{10}$th the nose radius. It is possible to optimize the nose and shoulder radii for the Microprobe mission, but these previously used ratios appear adequate, and their selection allows the use of an extensive body of existing aerodynamic data. The geometry of the Pioneer Venus small probes is shown in Fig. 3.

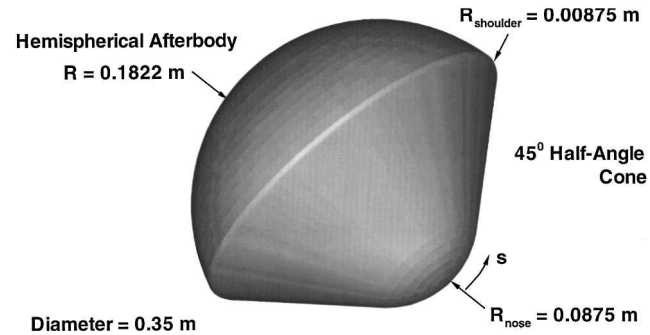

Fig. 4 Mars Microprobe aeroshell geometry.

Microprobe's hemispherical afterbody serves two purposes. First, because the vehicle's initial attitude is tumbling, it may encounter the atmosphere while traveling backward. A hemispherical afterbody with its center at the vehicle's center of gravity is not stable at this backward orientation and will foster rotation to a forward-facing attitude. Second, the shape has been shown to decrease the dynamic instability observed in blunt vehicles traversing the transonic flight regime.[7] Selection of the large hemispherical afterbody for Microprobe does not rely on previous mission's designs, but is similar to the one used in the Planetary Atmospheric Entry Test experiment.[8]

Regarding the backward stability issue, Pioneer Venus, Galileo, Viking, and Mars Pathfinder were all hypersonically stable in either a forward or backward orientation. To avoid a backward entry, each was oriented nose first and spin stabilized to assure a nose-first attitude at atmospheric interface. Because spin stabilization is not an option for Microprobe, an afterbody that assures the vehicle does not trim in a rearward-facing attitude must be chosen.

The desired impact velocity of Mars Microprobe is just below Mach 1. Unfortunately, aeroshells such as the 45- and 70-deg blunted cones mentioned suffer a dynamic instability at small angles of attack in the Mach 1.0–2.0 range.[2,7,9] That is, though they remain statically stable as they traverse that Mach range, an increase in incidence angles is observed. Because the instability is restricted to angles of attack less than 5 deg, the increase in incidence is bounded and results in a wobbling motion. Unfortunately for Microprobe, surface impact near Mach 1.0 means this instability interferes with its requirement of small angle of attack at impact. Both Viking and Mars Pathfinder deployed parachutes at supersonic speeds to avoid this dynamics problem. Galileo unexpectedly traversed the transonic flight regime, and flight data indicate a growth in incidence angles beginning at Mach 2.0 and increasing to a maximum value near 15 deg at Mach 1.0.

The source of the dynamic instability is still debated. Sammonds[7] argued that a hemispherical afterbody centered about the center of gravity would eliminate this problem because afterbody pressure forces would be directed through the c.g. such that asymmetric pressure distributions there would produce no pitching motions. He demonstrated this at Mach numbers up to 1.2. Whereas it is unproven for larger Mach numbers, it is arguable that a hemispherical afterbody will decrease the dynamic instability.

Based on the preceding discussion, the forebody geometry of the Mars Microprobe is specified to be a 45-deg sphere-cone with $R_n = 0.08125$ m, $R_s = 0.008125$ m, and $D = 0.325$ m. The afterbody shape is a hemispherical section with radius 0.174 m, which is centered about the expected c.g. location of the vehicle. The geometry is shown in Fig. 4.

Trajectory

Detailed analysis of the aerodynamics requires knowledge of the expected trajectory. A preliminary aerodynamic description of the Mars Microprobe was constructed using free-molecular aerodynamics, Newtonian aerodynamics, and Pioneer Venus supersonic and transonic wind-tunnel data. This description was then used in a preliminary six-DOF trajectory simulation to create an estimated nominal trajectory. Altitude and Mach number vs velocity from that trajectory are presented in Fig. 5. Points from this trajectory in each flight regime were then selected for more detailed analysis.

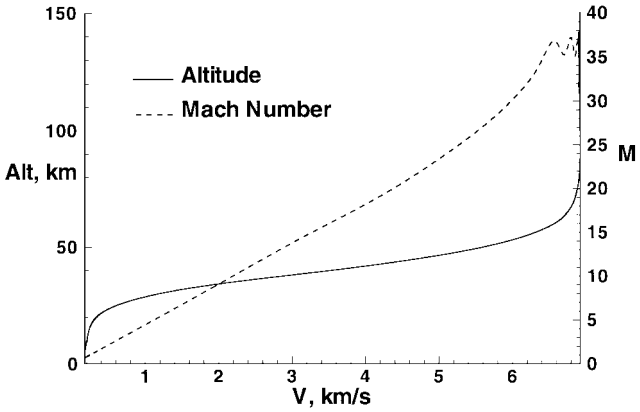

Fig. 5 Estimated Mars-entry trajectory.

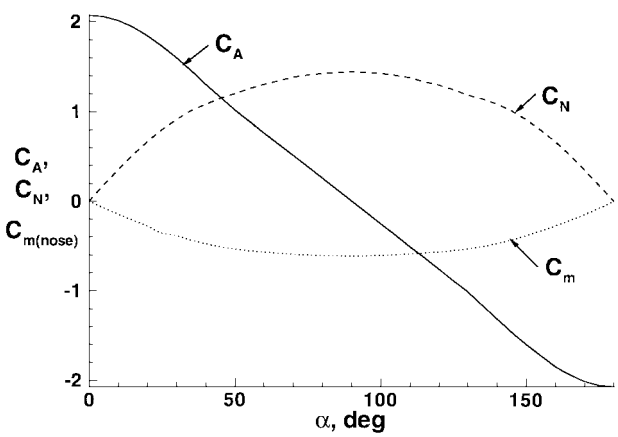

Fig. 6 Free-molecular flow aerodynamics.

Free-Molecular Flow

Free-molecular flow assumes there are no collisions between gas molecules in the flowfield. The surface is impacted by freestream particles, which are diffusely reflected after full thermal accommodation. Unlike hypersonic-continuum aerodynamics, where forces exerted on the body are primarily the integrated effect of surface pressures, free-molecular flow aerodynamics contain a significant contribution from shear stress.

The two Mars Microprobes are to be released from the host spacecraft 3 min prior to atmospheric interface. As the tumbling spacecraft approach the outer reaches of the atmosphere, they will encounter widely spaced molecules. Surface impacts of these molecules will exert the first aerodynamic forces on the entry vehicle. Knudsen number Kn is the ratio of the quiescent gas's mean free path to the vehicle's diameter. At the outer reaches of the atmosphere, Knudsen number is large. As long as it remains of order 10 or larger, the associated aerodynamic forces can be computed by free-molecular flow methods.

The free-molecular flow aerodynamics for the Mars Microprobe entry vehicles are presented in the form of nondimensional coefficients in Fig. 6. Because the geometry is axisymmetric, the static aerodynamics can be described by an axial force coefficient C_A, a normal force coefficient C_N, and a moment coefficient C_m. The reference area is the frontal area of the aeroshell (0.08296 m^2), and the reference length is the diameter (0.325 m). Unless otherwise specified, moments are taken about the actual nose of the vehicle. For a c.g. location 0.24D back from the nose or less, the vehicle is statically stable only when facing forward.

Hypersonic-Transitional and Continuum Aerodynamics

As the descent continues into the upper atmosphere, the mean free path (and Knudsen number) decrease, and collisions between particles must be accounted for in describing forces on the vehicles. This regime is the transitional flow regime. Even lower (below 55-km altitude for Microprobe), Knudsen number drops below 0.001, and continuum methods can be used to describe the flow about, and the forces on, the vehicle. Figure 7 presents Knudsen number Kn vs altitude for the high-altitude portion of the Microprobe trajectory.

Table 1 Axisymmetric results from DSMC

t, s	Alt, km	M	V, m/s	Kn	C_A
10.4	126.7	33.3	6909	86.5	2.054
20.3	113.2	35.1	6916	10.08	2.010
31.8	100.6	37.4	6921	1.25	1.901
38.0	91.4	39.1	6923	0.305	1.771
48.0	80.3	37.7	6908	5.46e−02	1.536
50.5	73.4	35.9	6884	2.45e−02	1.352
65.0	64.3	35.6	6751	6.78e−03	1.190
77.2	54.9	31.8	6168	1.83e−03	1.108

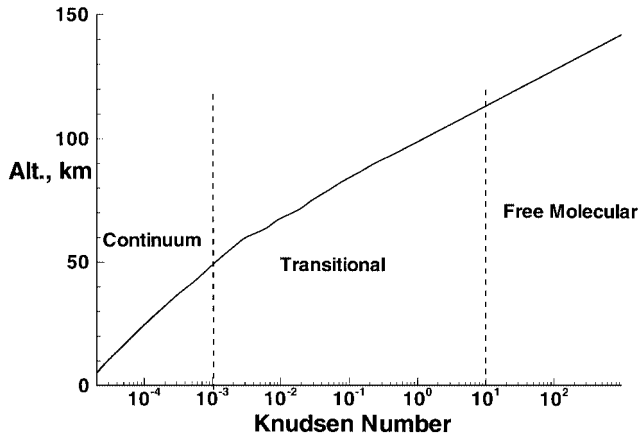

Fig. 7 High-altitude flight regimes.

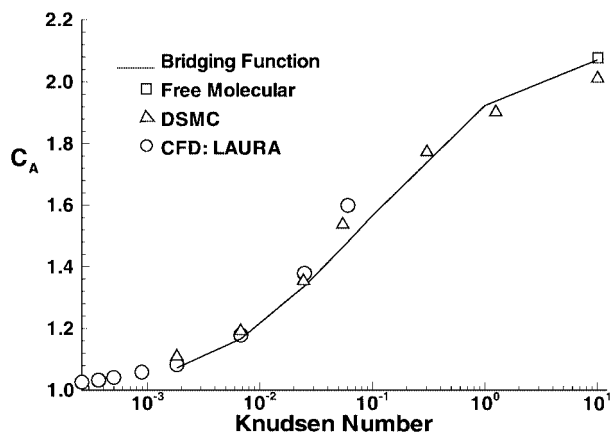

Fig. 8 Comparison of zero angle-of-attack axial force coefficients in the transitional flow regime.

The transitional aerodynamics for Microprobe were computed using DSMC methods and are discussed in Ref. 10. Eight axisymmetric solutions from that study are presented in Table 1, and seven of the points are plotted in Fig. 8. Figure 8 contains the free-molecular prediction, a bridging function estimate, and eight continuum CFD solutions discussed later. Transitional normal force coefficients and stability are discussed in Ref. 10.

In the hypersonic continuum regime, the LAURA CFD tool can describe the static aerodynamics of Microprobe. LAURA is an upwind-biased, point-implicit relaxation algorithm[11] for obtaining the numerical solution to the Navier–Stokes equations for three-dimensional viscous hypersonic flows in thermochemical nonequilibrium. The Mars atmosphere version of the code[12] contains an eight-species CO_2−N_2 chemical-kinetics model. This computational tool was used to describe the aerodynamics of Mars Pathfinder.[13,14] Predictions from the code have been shown to be in excellent agreement with the Mars Pathfinder flight data.[15]

LAURA solutions are computed at eight points in the trajectory's hypersonic continuum regime. Table 2 presents the 0-deg

Table 2 Axisymmetric results from LAURA CFD

t, s	Alt, km	M	V, m/s	Kn	C_A
48	80.5	37.7	6913	6.1e−02	1.598
55	73.4	35.9	6884	2.5e−02	1.378
72	55.8	32.8	6271	2.0e−03	1.086
82	48.7	25.9	5419	1.0e−03	1.061
92	43.3	19.9	4327	6.2e−04	1.049
116	34.9	10.0	2206	2.6e−04	1.027
125	32.6	7.5	1665	2.1e−04	1.028
142	29.5	5.0	1121	1.6e−04	1.035

Table 3 Three-dimensional results from LAURA, $\alpha = 10$ deg

t, s	M	C_A	C_N	C_m
72	32.8	1.0281	0.1687	−0.1106
82	25.9	1.0353	0.1689	−0.1103
92	19.9	1.0141	0.1706	−0.1125
116	10.0	1.0016	0.1691	−0.1115
126	7.5	0.9987	0.1668	−0.1125
142	5.0	1.0133	0.1635	−0.1064

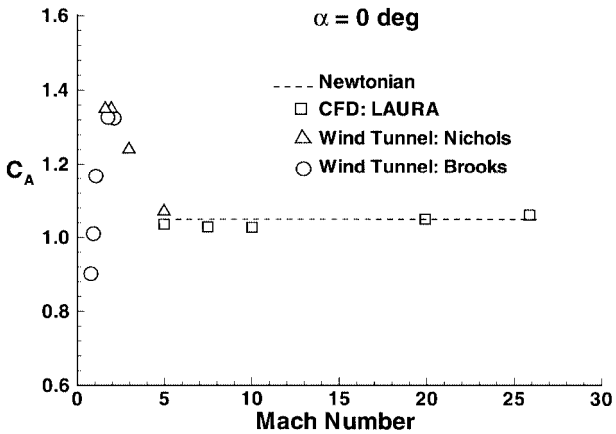

Fig. 9 Variation of axial force coefficients in the hypersonic flow regime.

angle-of-attack C_A results (also shown in Fig. 8). Additional forebody solutions are computed at 10-deg angle of attack for six of these trajectory points. Those results are listed in Table 3.

The variation in axial coefficient at 0-deg angle of attack across the hypersonic-continuum regime is presented in Fig. 9. Little change in C_A occurs across the Mach range. The variation at 10-deg angle of attack of the normal force and moment coefficients are given in Figs. 10 and 11. Again, the aerodynamic coefficients vary little down to Mach 5. (The aerodynamics below Mach 5 are discussed in subsequent sections.) The values predicted from the Newtonian flow approximation are included in Figs. 9–11. Newtonian flow assumes that the freestream flow is turned parallel to the surface. Local pressure is then a function only of the local surface inclination relative to the freestream. Whereas the simple Newtonian assumption agrees with the CFD predictions for the axial and normal force coefficients across the hypersonic regime, it underpredicts the absolute value of the moment coefficient by as much as 14%.

At the higher Mach numbers, the bow shock is sufficiently energetic to initiate dissociation of the triatomic CO_2 molecule. The degree of CO_2 dissociation on the stagnation streamline associated with four LAURA solutions is shown in Fig. 12. At Mach 33, CO_2 dissociates from its freestream mass fraction of 0.97–0.19 at the edge of the boundary layer. (The fully catalytic wall boundary condition forces complete recombination of the dissociated molecules.) Lesser degrees of dissociation occur with decreasing Mach number. No dissociation is predicted at Mach 10. When dissociation occurs, the residence time of the gas across the thin shock layer is insufficient to allow the gas to equilibrate. This phenomenon is a result of the small length scales associated with Microprobe. There does not

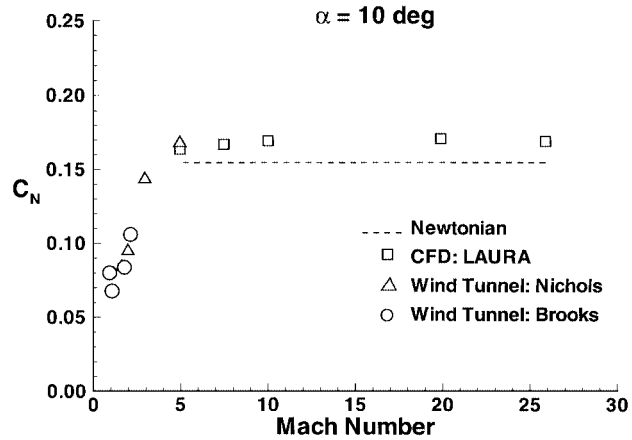

Fig. 10 Variation of normal force coefficients in the hypersonic flow regime.

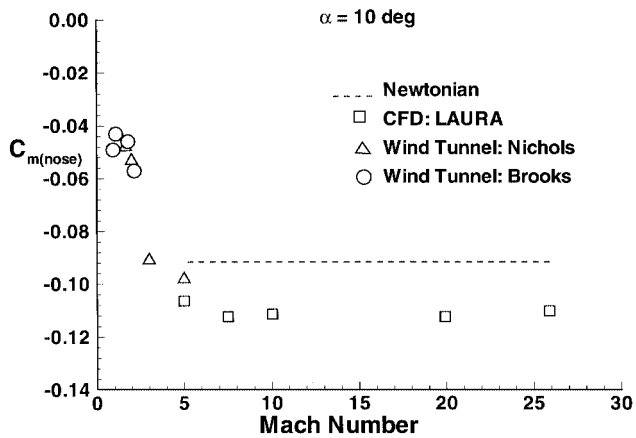

Fig. 11 Variation of the moment coefficient in the hypersonic flow regime.

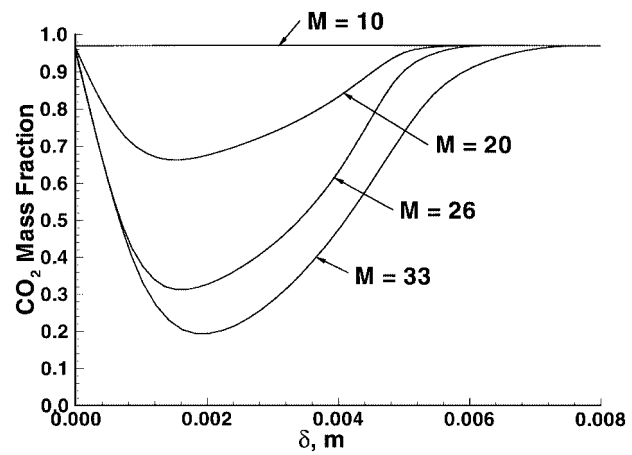

Fig. 12 Stagnation line profiles of CO_2 at hypersonic flow conditions.

appear to be a Mach range where an equilibrium gas assumption would be useful in predicting the flowfield about Microprobe.

Figure 12 also shows the associated shock standoff distances (indicated by that point where CO_2 dissociation begins). The distance at Mach 33 is large due to rarefaction effects; the standoff distance reaches a minimum below Mach 26, then grows with decreasing speeds.

Supersonic Aerodynamics

In the supersonic regime, existing wind-tunnel data may be used to describe the aerodynamics. Nichols and Nierengarten[6] tested 45-deg half-angle cones in the Jet Propulsion Laboratory (JPL) 21-in. supersonic wind tunnel at Mach 3.0, 2.0, and 1.65 and in the

JPL 20-in. hypersonic wind tunnel at Mach 5.0. The tests were performed in air at Reynolds number (based on diameter of 3.0-in. models) of 0.3×10^6 in the hypersonic tunnel and 1.0×10^6 in the supersonic tunnel. The flight Reynolds numbers expected for Mars Microprobe in this speed range are below 0.1×10^6 in the Mars CO_2 atmosphere. Whereas the flow in this regime should be that of a perfect gas, the ratio of specific heats for air at 1.4 is higher than the Mars atmosphere value of 1.33. In addition, these measurements examined a model that did not include the hemispherical afterbody. Afterbody effects are negligible for small angles of attack above Mach 5 (which allowed the forebody-only CFD used in the hypersonic aerodynamics description). Below Mach 5, however, the afterbody's influence increases. As shown in Figs. 9–11, the Mach 5 measurements compare well with the LAURA CFD calculations.

Figures 13–15 focus on the Mach range below 5 and include wind tunnel, ballistic range, and CFD data. The solid line in Figs. 13–15 labeled database is included to show trends across the Mach range. Figures 13–15 reveal a marked change in the aerodynamics across the supersonic and transonic regimes. The change is a result of the sonic line shifting from the nose region to the shoulder region. At Mach 5, the subsonic bubble remains on the spherical nose even at 10-deg incidence. By Mach 2, the sonic line has shifted to the shoulder even at 0-deg incidence. At this condition, the entire forebody shock layer is subsonic flow.

Pressure distributions and aerodynamic forces are affected by the sonic character of the shock layer. When the latter above the flank is supersonic, the pressure distributions there are flat (a characteristic of conical flow). When the shock layer is subsonic, the elliptic nature of the flow results in higher, more rounded pressure distributions. The net effect on the resulting forces is that the axial force increases while normal force and moment coefficients decrease. This combination results in a decrease in the static stability margin of the vehicle.

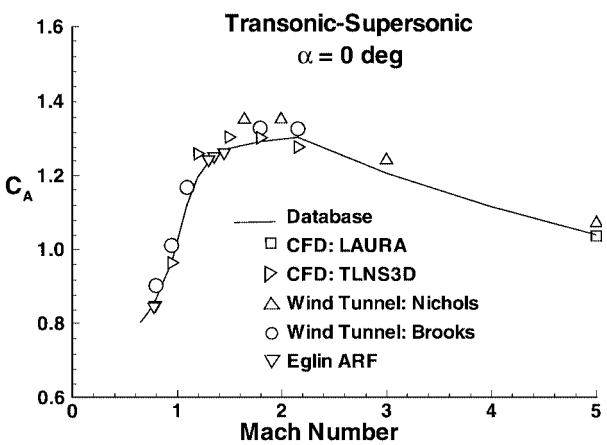

Fig. 13 Comparison of axial force coefficient predictions in the transonic and subsonic regimes.

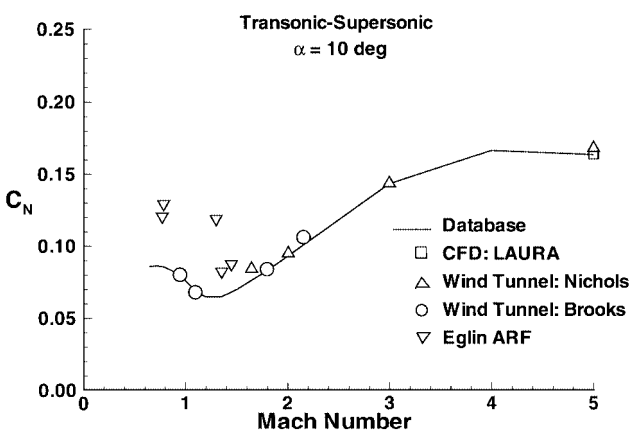

Fig. 14 Comparison of normal force coefficient predictions in the transonic and subsonic regimes.

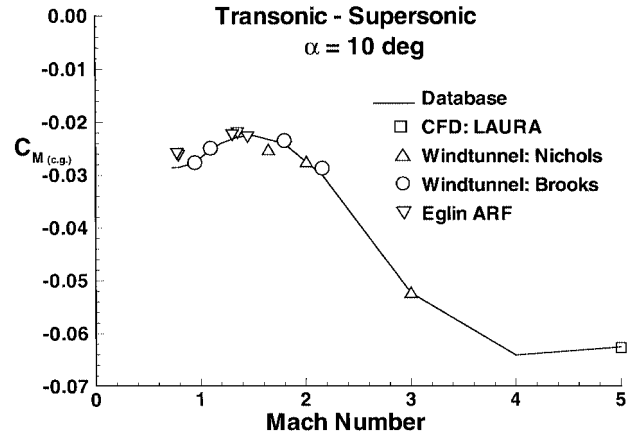

Fig. 15 Comparison of the moment coefficient predictions in the transonic and subsonic regimes.

If the vehicle's c.g. does not lie on the geometric symmetry line, the vehicle will trim at a nonzero angle of attack. As the Mach range between 5 and 2 is traversed, the decrease in static stability would introduce pitching motions for such an offset c.g. because the vehicle would then trim at a larger angle of attack. Because Microprobe has strict requirements on angle of attack at impact (and impact occurs shortly after traversing this Mach range), c.g. offset should be minimized to avoid the introduction of pitching motions late in the trajectory.

Transonic Aerodynamics

Figures 13–15 also contain the transonic aerodynamics. The probe's impact speed at just below Mach 1 and its requirement that this impact occur while at small angle of attack demand the best possible description of the aeroshell's aerodynamics in this speed regime. Unfortunately, transonic aerodynamics are complex, and testing and computations are difficult (as well as expensive). The description of Microprobe's transonic aerodynamics combines existing wind-tunnel data, new CFD, and recent ballistic-range tests performed for Microprobe.

Wind-tunnel data[2,16] in the transonic regime were obtained in support of the Pioneer Venus small probes, which have the same forebody as Microprobe. Both vehicles have hemispherical afterbodies (Figs. 3 and 4), though Microprobe's is larger. In Ref. 16, static aerodynamics for Pioneer Venus models were measured at Mach 0.2, 0.5, 0.8, 0.95, 1.1, 1.2, and 1.35 in the NASA Langley Research Center's 8-ft transonic wind tunnel and Mach 1.5, 1.8, and 2.16 in the NASA Langley Research Center Unitary Plan wind tunnel. Reference 16 describes testing problems encountered at Mach numbers 1.2, 1.35, and 1.5. Figures 13–15 exclude the data from those Mach numbers.

Figure 13 also contains CFD results at five points between Mach 0.6 and Mach 2.2 using the TLNS3D code.[17] These calculations are about the Microprobe geometry for conditions coincident with Brooks[16] wind-tunnel data. The results presented were preceded by an extensive grid-resolution study to resolve the wake region. The CFD calculations span the range where the Brooks study encountered problems with reflected wall–shock interactions. In an effort to assess the usefulness of the Pioneer Venus wind-tunnel measurements in the transonic regime, additional TLNS3D CFD was computed at the same five conditions for the Pioneer Venus geometry. The axial force coefficients for the two geometries are compared in Fig. 16. Higher base pressures on the large Microprobe afterbody result in a decrease (as large as 6%) in the predicted drag coefficient for the Microprobe geometry relative to the Pioneer Venus geometry.

Ballistic-range tests of the Microprobe geometry were performed at the U.S. Air Force Wright Laboratory's Aeroballistic Research Facility (ARF) at Eglin Air Force Base. The test were concentrated around Mach 0.8 and 1.4. The primary goal of these tests were to establish the dynamic stability of the vehicle (discussed in the next section). Static aerodynamics, however, were also measured and are

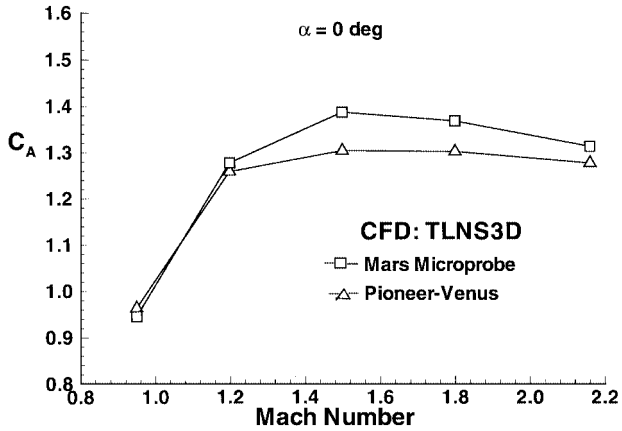

Fig. 16 Comparison of the TLNS3D CFD predictions for axial force coefficient on different afterbodies.

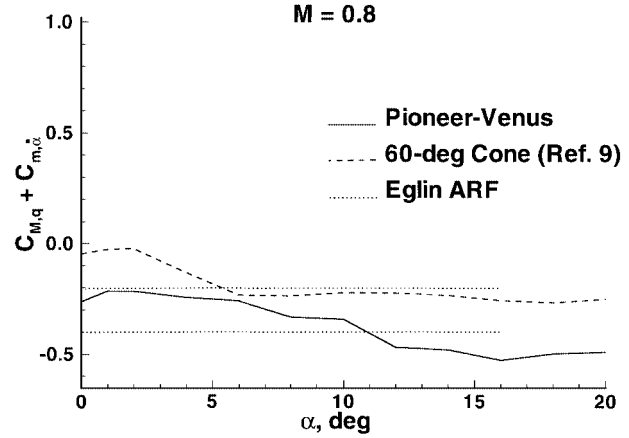

Fig. 17 Comparison of dynamic derivatives in the transonic regime, $M = 0.8$.

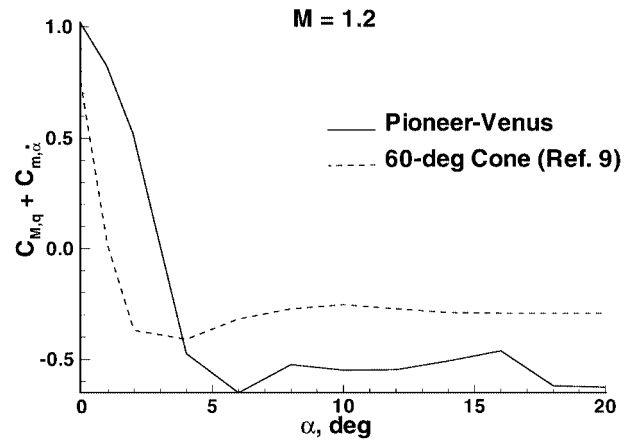

Fig. 18 Comparison of dynamic derivatives in the transonic regime, $M = 1.2$.

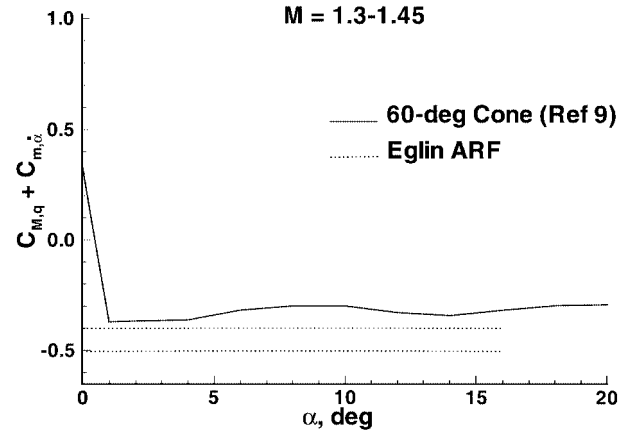

Fig. 19 Comparison of dynamic derivatives in the transonic regime, $M = 1.3$–1.45.

included in Figs. 13–15. With the exception of C_N, there is good agreement among the ballistic-range measurements, the CFD, and the wind-tunnel data. The ballistic range is accurate at measuring axial forces, it has difficulty resolving the small normal forces associated with a blunt body such as Microprobe.

The Reynolds numbers based on diameter for this wind-tunnel and ballistic-range data is between 0.5 and 3.0×10^6. The expected flight conditions have Reynolds numbers between 5×10^4 and 1×10^5 for this speed range.

Dynamic Derivatives

Detailed measurement of the dynamic derivatives for Microprobe over its entire trajectory to a level of accuracy necessary for precise six-DOF simulation is difficult given the time and cost restraints on the project. Microprobe must impact the surface while flying at small angle of attack. This impact will occur around Mach 0.8. The primary concern for dynamic stability, therefore, is in the transonic flight regime. Through use of existing data measured for the Mars Viking and Pioneer Venus missions in conjunction with the transonic dynamic data measured in the ARF ballistic range, an assessment of the transonic dynamic stability of Microprobe can be made.

In preparation for the Mars Viking mission, Uselton et al.[9] performed extensive wind-tunnel measurements of the dynamic stability of 60- and 70-deg half-angle cones using a forced-oscillation technique. Reference 9 concludes there is no appreciable difference between the dynamic response of the two cones when the c.g. location of the 70-deg cone is more forward than that of the 60-deg cone. Reference 9 also observes a decrease in dynamic stability for a given cone angle when the c.g. is moved farther from the nose. Based on these two observations, it is arguable that the 60-deg cone is a more dynamically stable shape than the 70-deg cone, but this increase in stability can be offset by an aft shift in the c.g. If this reasoning is extrapolated to 45-deg cones, a 45-deg cone should exhibit more dynamic stability than a 60-deg cone. Therefore, the Uselton et al.[9] 60-deg cone data should represent a conservative description of the dynamic performance of Microprobe. Figures 17–19 present the angle-of-attack variation of the dynamic derivatives at three Mach numbers in the transonic regime. Because the geometry is symmetric, the dynamic derivatives can be specified by a single parameter $(C_{m,q} + C_{m,\dot{\alpha}})$.

Dynamic tests in support of Pioneer Venus were performed in the Langley 8-ft transonic wind tunnel using a similar forced-oscillation technique.[4] The Pioneer Venus small probe geometry (Fig. 3) has the same forebody as Microprobe. The c.g. location is $0.22D$ back from the nose for the Pioneer Venus tests. Those tests were restricted to Mach numbers below 1.3 and so representative values are included only in Figs. 17 and 18.

Figures 17 and 19 also contain the ARF ballistic-range data for the two Mach numbers (0.8 and 1.4) examined. The ballistic range did not distinguish an angle-of-attack variation in the dynamic damping; those results (two separate measurements for each Mach number) are presented as the straight dotted lines in Figs. 17 and 19.

At Mach 0.8 (Fig. 17), all three data sources predict dynamic stability (a negative quantity) across the angle-of-attack range. Figure 17 shows that a 45-deg cone possess a higher degree of dynamic stability than the 60-deg cone. The ARF data are in good agreement with the wind-tunnel data.

The instability at small angles of attack for Mach 1.2 and 1.4 is indicated by the positive values for $(C_{m,q} + C_{m,\dot{\alpha}})$ in Figs. 18 and 19. The ARF ballistic-range data at Mach 1.3–1.45 did not detect a transonic dynamic instability for the Microprobe geometry. This increased stability may be due to Microprobe's hemispherical afterbody, which, as reported by Sammonds,[7] can eliminate or reduce the transonic dynamic instability.

Accurate six-DOF simulation over the entire entry trajectory requires knowledge of the dynamics at higher speeds. The Uselton

et al.[9] measurements are restricted to Mach numbers at 3.0 and below. For larger Mach numbers, other ballistic-range tests on blunt bodies[18] do not discern significant changes with Mach number. Thus, Mach 3.0 values for a 60-deg cone could be used as representative of the higher speed performance. Past experience with six-DOF simulations have also indicated that large variations in the dynamic derivatives at the higher Mach numbers have little effect on the hypersonic flight dynamics of the vehicle.

As with the supersonic and transonic data, there is a large difference between the Reynolds numbers for the dynamic data discussed and the expected flight values for Microprobe. Uselton et al.[9] examined Reynolds number effects on dynamic stability for 70-deg cones. No clear trend was revealed.

Conclusions

Selection of the aeroshell for Mars Microprobe involved consideration of the unique objectives of the mission. An enclosure was required that possessed the appropriate drag and stability characteristics to safely deliver the penetrator payload through entry to impact with the surface. A 45-deg half-angle cone with rounded nose and shoulder was shown to be a suitable candidate for the forebody shape. A hemispherical afterbody centered about the vehicle's c.g. location was chosen for the afterbody.

The aerodynamics of this aeroshell are discussed in each of the expected flight regimes during its Mars entry. This description makes use of DSMC analyses, CFD, existing wind-tunnel data, and new ballistic-range data.

Free-molecular flow aerodynamics indicate that the vehicle is statically unstable backward. If the tumbling vehicle has a rearward orientation when it encounters the atmosphere, it will reorient itself to a forward-facing attitude.

In the high-altitude transitional flow regime, a bridging function is shown to approximate the variation of the aerodynamic coefficients from their free-molecular values (at $Kn = 10.0$) to their hypersonic continuum values ($Kn = 0.001$). In addition, good agreement between CFD and DSMC predictions for axial coefficient is observed for $2.0 \times 10^{-3} \leq Kn \leq 3.0 \times 10^{-2}$.

In the hypersonic-continuum regime, the Newtonian assumption is shown to be a fair estimate for the axial and normal force coefficients for angles of attack up to 10 deg, but it underpredicts the magnitude of the moment coefficient by as much as 14%.

In the hypersonic regime, the small length scales associated with the forebody shock layer are insufficient to allow the dissociation of CO_2 to reach completion. Accurate description of the species profiles requires inclusion of chemical nonequilibrium effects for all cases in which chemical reactions occur. At Mach 10 and below, no CO_2 dissociation is predicted.

Around Mach 5, the sonic line shifts from the nose to the shoulder, which results in an increase in axial coefficient and a decrease in static stability of the vehicle.

Ballistic-range tests reveal that the combination of 45-deg cone, forward c.g. location, and hemispherical afterbody has reduced the dynamic instability often suffered by large-angle cones traversing the transonic flow regime.

Acknowledgments

Thanks are extended to Eric Slimko of the Jet Propulsion Laboratory for many helpful discussions. Didier Rault of NASA Langley Research Center provided the free-molecular flow aerodynamics presented herein.

References

[1]Braun, R. D., Mitcheltree, R. A., and Cheatwood, F. M., "Mars Microprobe Entry-to-Impact Analysis," *Journal of Spacecraft and Rockets*, Vol. 36, No. 3, pp. 412–420; also *Proceedings from the 1997 IEEE Aerospace Conference*, 1997.

[2]Kirk, D. B., Intrieri, P. F., and Seiff, A., "Aerodynamic Behavior of the Viking Entry Vehicle: Ground Test and Flight Results," *Journal of Spacecraft and Rockets*, Vol. 15, No. 4, 1978, pp. 208–212.

[3]Spear, A. J., Freeman, D. C., and Braun, R. D., "Mars Pathfinder Status at Launch," International Astronautical Federation, IAF Paper 96-Q.3.02, Beijing, PRC, Oct. 1996.

[4]Weinberg, S. A., "Final Data Report—Pioneer–Venus Static and Dynamic Transonic Wind Tunnel Tests," General Electric Corp., 9154-TDM-75-013, Valley Forge, PA, July 1975.

[5]Moss, J. N., LeBeau, G. J., Blanchard, R. C., and Price, J. M., "Rarefaction Effects on the Galileo Probe Aerodynamics," *20th International Symposium on Rarefied Gas Dynamics,* edited by C. Shen, Peking Univ. Press, Beijing, PRC, 1997, pp. 495–500.

[6]Nichols, J. O., and Nierengarten, E. A., "Aerodynamics Characteristics of Blunted Bodies," Jet Propulsion Lab., TR 32-677, California Inst. of Technology, Pasadena, CA, Feb. 1964.

[7]Sammonds, R. I., "Dynamics of High Drag Probe Shapes at Transonic Speeds," NASA TN-D-6489, Sept. 1971.

[8]Seiff, A., Reese, D. E., Sommer, S. C., Kirk, D. B., Whiting, E. E., and Niemann, H. B., "PAET, An Entry Probe Experiment in the Earth's Atmosphere," *Icarus*, Vol. 18, No. 4, 1973, pp. 525–563.

[9]Uselton, B. L., Shadow, T. O., and Mansfield, A. C., "Damping in Pitch Derivatives of 120 and 140 Deg Blunted Cones at Mach Numbers 0.6 Through 3.0," U.S. Air Force, Arnold Engineering Development Center, TR-70-49, Arnold Air Force Station, TN, April 1970.

[10]Moss, J. N., Wilmoth, R. G., and Price, J. M., "Direct Simulation Monte Carlo Calculations of Aerothermodynamics for Mars Microprobe Capsules," *Journal of Spacecraft and Rockets*, Vol. 36, No. 3, 1999, pp. 399–404.

[11]Gnoffo, P. A., "An Upwind-Biased, Point-Implicit Relaxation Algorithm for Viscous, Compressible Perfect-Gas Flows," NASA TP-2953, Feb. 1990.

[12]Mitcheltree, R. A., "Aerothermodynamic Methods for a Mars Environmental Survey Mars Entry," *Journal of Spacecraft and Rockets*, Vol. 31, No. 3, 1994, pp. 516–523.

[13]Braun, R. D., Powell, R. W., Engelund, W. C., Gnoffo, P. A., Weilmuenster, K. J., and Mitcheltree, R. A., "Mars Pathfinder Six-Degree-of-Freedom Entry Analysis," *Journal of Spacecraft and Rockets*, Vol. 32, No. 6, 1996, pp. 993–1000.

[14]Gnoffo, P. A., Weilmuenster, K. J., Braun, R. D., and Cruz, C. I., "Influence of Sonic Line Location on Mars Pathfinder Aerodynamics," *Journal of Spacecraft and Rockets*, Vol. 33, No. 2, 1996, pp. 169–177.

[15]Gnoffo, P. A., Braun, R. D., Weilmuenster, K. J., Mitcheltree, R. A., Engelund, W. C., and Powell, R. W., "Prediction and Validation of Mars Pathfinder Hypersonic Aerodynamic Data Base," AIAA Paper 98-2445, June 1998.

[16]Brooks, J. D., "Some Anomalies Observed in Wind Tunnel Tests of a Blunt Body at Transonic and Supersonic Speeds," NASA TN-D-8237, June 1976.

[17]Vatsa, V. N., Turkel, E., and Abolhassani, J. S., "Extension of Multigrid Methodology to Supersonic/Hypersonic 3-D Viscous Flows," NASA CR-187612, Aug. 1991.

[18]Krumins, M. V., "A Ballistic Range Study of the Aerodynamic Characteristics of Mars Probe/Lander Shapes," AIAA Paper 67-167, Jan. 1967.

R. D. Braun
Guest Editor